About Darcy's law in non-Galilean frame

Christian Geindreau, E. Sawicki, Jean-Louis Auriault, Pascale Royer

About Darcy's law in non-Galilean frame

C. Geindreau *, E. Sawicki, J.-L. Auriault and P. Royer

SUMMARY

This paper is aimed towards investigating the filtration law of an incompressible viscous Newtonian fluid through a rigid non-inertial porous medium (e.g. a porous medium placed in a centrifuge basket). The filtration law is obtained by upscaling the flow equations at the pore scale. The upscaling technique is the homogenization method of multiple scale expansions which rigorously gives the macroscopic behaviour and the effective properties without any prerequisite on the form of the macroscopic equations. The derived filtration law is similar to Darcy's law, but the tensor of permeability presents the following remarkable properties: it depends upon the angular velocity of the porous matrix, it verifies Hall–Onsager's relationship and it is a non-symmetric tensor. We thus deduce that, under rotation, an isotropic porous medium leads to a non-isotropic effective permeability. In this paper, we present the results of numerical simulations of the flow through rotating porous media. This allows us to highlight the deviations of the flow due to Coriolis effects at both the microscopic scale (i.e. the pore scale), and the macroscopic scale (i.e. the sample scale). The above results confirm that for an isotropic medium, phenomenological laws already proposed in the literature fails at reproducing three-dimensional Coriolis effects in all types of pores geometry. We show that Coriolis effects may lead to significant variations of the permeability measured during centrifuge tests when the inverse Ekman number Ek^{-1} is $\mathcal{O}(1)$. These variations are estimated to be less than 5% if $\mathsf{Ek}^{-1} < 0.2$, which is the case of classical geotechnical centrifuge tests. We finally conclude by showing that available experimental data from tests carried out in centrifuges are not sufficient to determining the effective tensor of permeability of rotating porous media.

KEY WORDS: filtration law; porous media; rotating; upscaling; homogenization; centrifuge

1. INTRODUCTION

The focus of the present study is on the fundamentals of fluid flow in rotating rigid porous media. In the absence of external forces, the steady-state slow flow of an incompressible liquid through a rigid inertial porous matrix is described by the well-known Darcy's law:

$$\mathbf{v} = -\frac{\mathbf{K}}{\mu}(\nabla p - \rho \mathbf{g}), \quad v_i = -\frac{K_{ij}}{\mu}\left(\frac{\partial p}{\partial X_j} - \rho g_j\right) \tag{1}$$

where the tensor of intrinsic permeability $\mathbf{K}$ (m^2) is a positive and symmetrical tensor, the vector $\mathbf{v}$ represents the Darcy velocity, μ is the dynamic fluid viscosity and ∇p denotes the macroscopic pressure gradient, which forces the flow through the porous matrix, ρ is the fluid density and $\mathbf{g}$ is the vector of gravity acceleration. The description is completed by the volume balance

$$\nabla \cdot \mathbf{v} = 0, \quad \frac{\partial v_i}{\partial X_i} = 0 \tag{2}$$

The purpose of this paper is to consider the steady-state slow flow of an incompressible liquid through a non-inertial rigid porous matrix. As an example, we will consider the flow through a porous sample placed in the basket of a centrifuge, of angular velocity $\boldsymbol{\omega}$ with respect to a Galilean frame. The issue is to determine the consequences of the angular velocity $\boldsymbol{\omega}$ on Darcy's law (1).

It is worth keeping in mind that Darcy's law (1) was obtained from experiments conducted on Earth surface, which is itself submitted to rotation. However, as it will be shown later, for classical soils Earth rotation is sufficiently low to ensure that there is no rotation effect on the filtration law. Under such circumstances, Earth can be seen as a Galilean frame.

In available centrifuge tests, the porous samples are assumed to be isotropic. There exist two phenomenological filtration laws for modelling the flow of water through a rotating porous medium. The first model, see, e.g. [1, 2] is based upon Darcy's law formulation (1) with a modified hydraulic conductivity k^{cen}

$$k^{\mathrm{cen}} = kN^x \tag{3}$$

In the above expression, k (m/s) denotes the scalar hydraulic conductivity of the isotropic porous medium under zero angular rotation. The dimensionless parameter N is such that Ng represents the acceleration level which has been reached during the test. It is shown that the exponent x varies with respect to N. Experimental data confirm the N-dependence of k^{cen} [2]. Let us remark that the definition of the hydraulic conductivity k^{cen} is not clear and different points of view can be found in the literature [3, 4]. In the following, we prefer to work with the permeability K (m^2) to avoid any misunderstanding.

The second existing model [5] is based upon the conjecture that Coriolis effects should explicitly be accounted for. Based on a phenomenological reasoning, the resulting dimensionless filtration law for an isotropic porous media reads

$$\mathbf{v} = -\frac{K}{\mu}(\nabla p + \mathsf{Ek}^{-1}\mathbf{e}_\omega \times \mathbf{v}) \tag{4}$$

where $\mathbf{v}$ is the flow rate vector, K represents the scalar permeability, ∇p denotes the pressure gradient (including centrifugal force), $\mathbf{e}_\omega$ is a unit vector in the direction of the rotational velocity and Ek is the Ekman number, that is, the ratio of the viscous term to Coriolis term in Navier–Stokes equations. Equation (4) can be rewritten into a Darcy's-type form (1)

$$\mathbf{v} = -\frac{\mathbf{K}^{\mathrm{phe}}}{\mu}\nabla p \tag{5}$$

in which $\mathbf{K}^{\mathrm{phe}}$ (m^2) is a non-symmetrical and ω-dependent permeability tensor and is given by

$$\mathbf{K}^{\mathrm{phe}} = [K^{-1}\mathbf{I} + \mathsf{Ek}^{-1}\mathbf{e}_\omega\times]^{-1} \tag{6}$$

On the other hand, by applying the theory of non-equilibrium thermodynamics [6] to the general problem of fluid flow in a rotating porous medium, it can be shown that the filtration law is of

Darcy's type (1), but that the tensor of permeability satisfies Hall–Onsager's property

$$K_{ij}(\boldsymbol{\omega}) = K_{ji}(-\boldsymbol{\omega}) \tag{7}$$

This latter property is the analogue for the permeability of a rotating porous medium of Hall's effect, which characterizes the conductivity of a material subject to a magnetic field. It should be noted that Onsager's relationship directly arises, on the basis of the principles of statistical mechanics, from the microscopic laws of particle motions, and by using the principle of time reversal invariance of these laws. Equation (7) tells us that when an isotropic porous medium is submitted to rotation, its tensor of effective permeability is no longer isotropic: $K_{ij} \neq K_{ji} \neq 0$ when $i \neq j$. It can easily be shown that the permeability tensor of the phenomenological model (6) verifies Hall–Onsager's property (7).

More recently, [7, 8], the filtration law in a rotating porous medium was derived by upscaling the pore-scale description. A deterministic upscaling technique was used, namely the homogenization method of multiple scale expansions. With regard to the research contributions reviewed above, the novel aspect of these works is that the filtration law is rigorously derived from the physics at the pore scale and that, furthermore, no specific geometry or isotropy property is at issue; it results in the most general filtration model at the Darcy scale, which takes form (1), but with a different permeability tensor $\mathbf{K}^{\mathrm{rot}}$.

Physical phenomena in heterogeneous systems such as porous media are homogenizable, i.e. may be modelled by means of an equivalent continuous macroscopic description, provided that the condition of separation of scales is satisfied [9, 10]. This fundamental condition may be expressed as

$$\varepsilon = \frac{l}{L} \ll 1 \tag{8}$$

in which l and L are the characteristic lengths of the heterogeneities (here, the pore characteristic size) and of the macroscopic sample or excitation, respectively. The macroscopic equivalent model is obtained from the description at the heterogeneity scale by Auriault [11]: (i) assuming the medium to be periodic, without loss of generality (see Section 2); (ii) writing the local description in a dimensionless form; (iii) estimating the order of magnitude of the dimensionless numbers with respect to the scale ratio ε; (iv) looking for the unknown fields in the form of asymptotic expansions in powers of ε; (v) solving the boundary-value problems that arise at the successive orders of ε after introducing the asymptotic expansions in the local dimensionless description. The macroscopic equivalent model is obtained from the compatibility conditions, which are the necessary conditions for the existence of the solutions to the boundary-value problems. Generally speaking, the main advantages of the method rely upon the possibility of: (a) avoiding prerequisites at the macroscopic scale; (b) modelling finite size macroscopic samples; (c) modelling macroscopically non-homogeneous media or phenomena; (d) modelling problems with several separations of scales; (e) modelling several simultaneous phenomena; (f) determining whether the system 'medium + phenomena' is homogenizable or not; (g) providing the domains of validity of the macroscopic models.

After underlining the equivalence between random and periodic media, we give a brief review of the derivation of Darcy's law by applying homogenization to Stokes equations at the pore scale. We then focus on the flow through a rotating porous matrix, e.g. through a sample placed in the basket of a centrifuge. The relative importance of Coriolis effects is measured by means of the inverse Ekman number, which is the ratio of the Coriolis term to the viscous term in the

Stokes equation: $\mathsf{Ek}^{-1} = 2\rho\omega l^2/\mu$, where μ and ρ denote the dynamic viscosity and the density of the fluid, respectively. As a typical example, we consider a centrifuge of angular velocity $\omega \sim 300$ rpm, and a liquid of viscosity $\mu \sim 10^{-3}$ Pa s and of density $\rho \sim 10^3$ kg/m^3. Using the size of grains as characteristic length l, the resulting values of the inverse Ekman number Ek^{-1} range from 62 for sands ($l \sim 10^{-3}$ m) to 6.2×10^{-5} for clays ($l \sim 10^{-6}$ m). Hence, we shall consider that the order of magnitude of the inverse Ekman number is such that $\mathsf{Ek}^{-1} = \mathcal{O}(1)$, which with respect to the scale ratio ε actually means $\varepsilon \ll \mathsf{Ek}^{-1} \ll \varepsilon^{-1}$. We then employ the homogenization method, which leads to a macroscopic filtration law of Darcy' type (1), but whose effective tensor of permeability $\mathbf{K}^{\mathrm{rot}}$ is non-symmetric and verifies Hall–Onsager's relationship (7). The homogenized tensor of permeability, which we compare to the above-cited models, clearly proves by its definition, that the deviations from Darcy's law are due to Coriolis forces. Rotation effects are twofold. Firstly, the centrifugal force increases the forcing term ∇p, which is the sought-after purpose in a centrifuge filtration test. Compared to a classical filtration test, this increased forcing term does not change the pore-scale velocity pattern: velocities are just everywhere increased by a constant ratio. Secondly, Coriolis forces deviates the pore-scale velocity field, which results in a rotation-dependent permeability. This second effect is present when the Ekman number is $\mathcal{O}(1)$.

We then present the results of numerical simulations carried out for the flow through rotating porous media at both the microscopic and the macroscopic scales. We first study the influence of Coriolis forces at the microscopic scale on the flow through a rotating periodic array of cylinders and spheres. This study represents an interesting first step toward understanding Coriolis effects on the flow through porous media. Deviations of the flow which are due to Coriolis forces, that is, to the angular velocity are clearly highlighted. Numerical results obtained for different values of the radius of cylinders (or spheres) and porosity are presented. They suggest that it is more pertinent to use the permeability to estimate the Ekman number and they confirm that the phenomenological model (6) fails at reproducing three-dimensional Coriolis effects in all types of pores geometry. Finally, numerical results of the flow through a permeameter placed in a centrifuge basket highlight that the macroscopic velocity is also deviated and the pressure field is not homogeneous. We finally show that Coriolis effects may lead to significant variations of the permeability K^{cen} (m^2) which can be measured during centrifuge test when the Ekman number is $\mathcal{O}(1)$. These variations are estimated to be less than 5% if $\mathsf{Ek}^{-1} < 0.2$, which is the case of classical geotechnical centrifuge tests [2].

2. RANDOM AND PERIODIC POROUS MEDIA

Consider a random inertial porous medium that fulfills the condition of separation of scales. Fluid flow through this porous medium can therefore be described by means of a continuous macroscopic description and there exists a representative elementary volume (REV), which we denote by Ω_{REV}, see Reference [12]. To a given degree of accuracy as the medium is random, the REV contains all the required information that permits to define the equivalent macroscopic medium. Let consider an orthotropic porous medium, which with regard to flow properties coincides with the most general case of anisotropy. Without loss of generality, we may choose the REV to be a parallelepiped whose edges are parallel to the orthotropy axes.

Let now construct a period Ω by introducing three successive plane symmetries with respect to three non-parallel faces of the REV. Both the resulting periodic medium of period Ω and the

random medium of REV Ω_{REV} have the same macroscopic description and their permeabilities present the same properties. There is, therefore, no loss of generality by considering a periodic medium, when looking for the general structure of the macroscopic behaviour.

3. DARCY'S LAW

In this section, we give a brief review of the investigation conducted in Reference [10], in which Darcy's law is rigorously derived by homogenization. Consider a porous medium of period Ω and bounded by $\partial\Omega$. Within the periodic cell, the fluid occupies the domain Ω_p, and the fluid–solid interface is denoted by Γ (Figure 1). We also assume the porous matrix to be rigid. Relatively to the Galilean porous matrix frame R_0, the momentum balance for the quasi-static flow of an incompressible viscous Newtonian liquid is given in each point M of the pore space by Stokes equation

$$\mu\nabla^2\mathbf{w} - \nabla p = \mathbf{0} \quad \text{in } \Omega_p \tag{9}$$

where the vector $\mathbf{w}$ is the fluid velocity relatively to the matrix frame, p denotes the pressure and μ represents the fluid viscosity. Gravitational Earth acceleration is included in the pressure term. To complete the pore-scale description we shall also consider the incompressibility condition and the no-slip condition on Γ

$$\nabla \cdot \mathbf{w} = 0 \quad \text{in } \Omega_p, \quad \mathbf{w} = \mathbf{0} \quad \text{on } \Gamma \tag{10}$$

3.1. Dimensionless pore-scale description

We use the local pore length scale l as the characteristic length scale of reference for normalizing the variations of the differential operators: in other words, we apply the so-called microscopic point of view [11]. Other characteristic quantities are denoted by using the subscript c. The pore-scale description introduces a single dimensionless number, Q, which represents the ratio of the pressure term to the viscous forces $Q = \bar{p}_c l/\mu w_c$, where $\bar{p}_c$ denotes the characteristic pressure

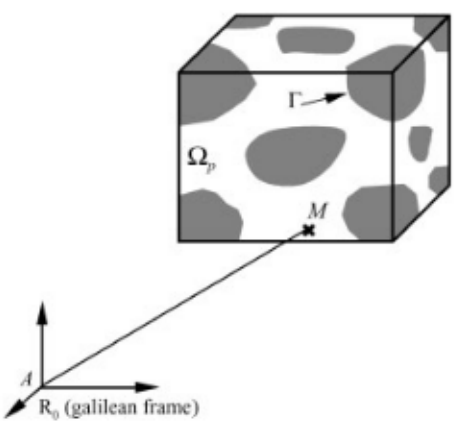

Figure 1. Scheme of the periodic cell Ω in a Galilean frame R_0.

increment applied to the sample. For estimating Q with respect to the scale ratio ε, we consider the following phenomenological argument: the local viscous flow is driven by a macroscopic pressure gradient [11]. In an order of magnitude sense, this argument reads $\mu w_c/l^2 = \mathcal{O}(\bar{p}_c/L)$. Therefore, we obtain

$$Q = \bar{p}_c l/\mu w_c = \mathcal{O}(\varepsilon^{-1}) \tag{11}$$

For simplicity we have kept, for the dimensionless variables, the same notations as for the original variables. The formal dimensionless set that describes the flow is thus written

$$\mu\nabla^2\mathbf{w} - Q\nabla p = \mathbf{0} \quad \text{in } \Omega_p \tag{12}$$

$$\nabla\cdot\mathbf{w} = 0 \quad \text{in } \Omega_p, \quad \mathbf{w} = \mathbf{0} \quad \text{on } \Gamma \tag{13}$$

3.2. Upscaling

We may now employ the homogenization procedure by firstly introducing the multiple scale coordinates [6, 12]: the macroscopic dimensionless space variable $\mathbf{x} = \mathbf{X}/L$ (where $\mathbf{X}$ represents the physical space variable) is related to the microscopic dimensionless space variable $\mathbf{y} = \mathbf{X}/l$ by $\mathbf{x} = \varepsilon\mathbf{y}$. Then, by applying the technique of multiple scale expansions, we may look for the velocity $\mathbf{w}$ and the pressure p in the form of asymptotic expansions of powers of ε

$$\mathbf{w} = \mathbf{w}^{(0)}(\mathbf{x},\mathbf{y}) + \varepsilon\mathbf{w}^{(1)}(\mathbf{x},\mathbf{y}) + \varepsilon^2\mathbf{w}^{(2)}(\mathbf{x},\mathbf{y}) + \cdots \tag{14}$$

$$p = p^{(0)}(\mathbf{x},\mathbf{y}) + \varepsilon p^{(1)}(\mathbf{x},\mathbf{y}) + \varepsilon^2 p^{(2)}(\mathbf{x},\mathbf{y}) + \cdots \tag{15}$$

Incorporating the above expansions in the set (12)–(13) and identifying at the successive orders of ε allows the construction of appropriate boundary-value problems. Solving these boundary-value problem leads to the macroscopic description.

The lowest order yields

$$\frac{\partial p^{(0)}}{\partial y_i} = 0, \quad p^{(0)} = p^{(0)}(\mathbf{x}) \tag{16}$$

Hence, the first-order pressure is constant over the period. Considering the next order, we obtain a boundary-value problem with respect to the first-order velocity $\mathbf{w}^{(0)}$ and to the second-order pressure $p^{(1)}$:

$$\mu\frac{\partial^2 w_i^{(0)}}{\partial y_j\partial y_j} - Q^*\frac{\partial p^{(0)}}{\partial x_i} - Q^*\frac{\partial p^{(1)}}{\partial y_i} = 0 \quad \text{in } \Omega_p \tag{17}$$

$$\frac{\partial w_i^{(0)}}{\partial y_i} = 0 \text{ in } \Omega_p, \quad w_i^{(0)} = 0 \quad \text{on } \Gamma \tag{18}$$

where $\mathbf{w}^{(0)}$ and $p^{(1)}$ are Ω-periodic and the quantity $Q^* = Q\varepsilon = \mathcal{O}(1)$.

A weak formulation of the above set is required for determining its solution, which as it will be seen later, is linked to the properties of the effective properties. For this purpose, we shall introduce the Hilbert space W of vectors $\mathbf{u}$ of Ω_p, that are Ω-periodic, divergence free and zero-valued over Γ. This Hilbert space is equipped with the following inner product:

$$(\mathbf{u},\mathbf{w})_W = \int_{\Omega_p}\frac{\partial u_i}{\partial y_j}\frac{\partial w_i}{\partial y_j}\,\mathrm{d}y \tag{19}$$

Let now multiply Equation (17) by $\mathbf{u} \in W$ and integrate it over Ω_p. Integrating by parts, applying the divergence theorem and then using the property of periodicity and the boundary condition on Γ, we obtain the following weak formulation:

$$\forall \mathbf{u} \in W, \quad \int_{\Omega_p} \mu \frac{\partial u_i}{\partial y_j} \frac{\partial w_i^{(0)}}{\partial y_j} \mathrm{d}y = - \int_{\Omega_p} Q^* u_i \frac{\partial p^{(0)}}{\partial x_i} \mathrm{d}y \tag{20}$$

The above formulation is strongly elliptic [13], and presents a unique solution $\mathbf{w}^{(0)}$ which is a linear function of $\partial p^{(0)}/\partial x_i$

$$w_i^{(0)} = -\frac{k_{ij}}{\mu} \frac{\partial p^{(0)}}{\partial x_j} \tag{21}$$

where the tensor field $\mathbf{k}$ is a function of $\mathbf{y}$. Finally, let consider the volume balance (13) at the second order

$$\frac{\partial w_i^{(1)}}{\partial y_i} + \frac{\partial w_i^{(0)}}{\partial x_i} = 0 \quad \text{in } \Omega_p \tag{22}$$

Integrating over Ω_p, we obtain

$$\frac{\partial v_i}{\partial x_i} = 0, \quad v_i = \langle w_i^{(0)} \rangle = -\frac{K_{ij}}{\mu} \frac{\partial p}{\partial x_j}, \quad K_{ij} = \langle k_{ij} \rangle = \frac{1}{\Omega} \int_{\Omega_p} k_{ij} \mathrm{d}y \tag{23}$$

which represents the macroscopic equivalent behaviour at the order $\mathcal{O}(\varepsilon)$ of approximation. The second equality in (23) represents Darcy's law.

3.3. *Comments*

The above derivation of Darcy's law conjures up the following comments:

- It can easily be proved that the tensor of permeability $\mathbf{K}$ is positive and symmetric [10]. It should be noted that both these properties directly arise from the weak formulation (20). The dimensional permeability $\mathbf{K}$ (m^2) characterizes the porous medium. It does not depend on the forcing macroscopic gradient of pressure ∇p.
- By definition, the macroscopic velocity $\mathbf{v} = \langle \mathbf{w}^{(0)} \rangle$ is a volume average velocity. It can, however, be shown that this volume average is equal to a surface average [11], which ascribes to $\mathbf{v}$ the required properties of a Darcy's velocity.
- The fact that $p^{(0)}$ is constant over the period tells us that the pressure keeps the same meaning at both the local scale and the macroscopic scale.
- Darcy's law appears to be the macroscopic momentum balance of the liquid flow through a Galilean porous matrix. As a consequence, in the case of a non-Galilean porous matrix, we may thus expect the momentum balance, that is, Darcy's law to be modified. This issue is the purpose of the next section.

4. FILTRATION LAW IN ROTATING POROUS MATRIX

The objective of the present section is the derivation by homogenization of the filtration law in a rotating porous medium. We apply the same methodology as in the preceding section; for details related to the analysis below, the reader is referred to References [7, 8].

Let now consider the flow through a porous medium placed in a centrifuge of radius r. Relatively to the moving porous matrix frame R_1 (see Figure 2), the momentum balance for the quasi-static flow of an incompressible viscous Newtonian liquid is now written as

$$\mu\nabla^2\mathbf{w} - \nabla p = \rho(\gamma_e + \gamma_c) \quad \text{in } \Omega_p \tag{24}$$

The vectors γ_e and γ_c represent the convective and the Coriolis accelerations, respectively, with respect to a Galilean frame (R_0)

$$\gamma_e = \gamma(O) + \frac{d\boldsymbol{\omega}}{dt} \times \mathbf{OM} + \boldsymbol{\omega} \times (\boldsymbol{\omega} \times \mathbf{OM}) \tag{25}$$

$$\gamma_c = 2\boldsymbol{\omega} \times \mathbf{w} \tag{26}$$

In the above equations, $\boldsymbol{\omega}$ denotes the angular velocity of the porous matrix (i.e. of the centrifuge), O is a fixed point of the porous matrix within the period and M represents a current point in Ω_p (Figure 2). To be completed, the local description also includes the incompressibility condition and the no-slip condition on Γ

$$\nabla \cdot \mathbf{w} = 0 \quad \text{in } \Omega_p, \quad \mathbf{w} = \mathbf{0} \quad \text{on } \Gamma \tag{27}$$

4.1. Dimensionless pore-scale description

We use again the local pore length-scale l as the characteristic length scale for normalizing the variations of the differential operators. Let us consider a centrifuge of radius r and whose constant angular velocity is $\boldsymbol{\omega} = \omega\mathbf{e}_\omega$, where ω is constant. From the pore-scale description arise four dimensionless numbers: the ratio Q, which has already been defined and estimated in the preceding section ($Q = \mathcal{O}(\varepsilon^{-1})$); the ratio R of the macroscopic convective inertia $\rho\gamma(O)$ to the viscous force $\mu\nabla^2\mathbf{w}$; the ratio A of the local convective inertia $\rho\boldsymbol{\omega} \times (\boldsymbol{\omega} \times \mathbf{OM})$ to the macroscopic convective inertia $\rho\gamma(O)$ and the Ekman number, Ek, the ratio of the viscous force $\mu\nabla^2\mathbf{w}$ to the Coriolis inertia $2\rho\boldsymbol{\omega} \times \mathbf{w}$. We have $A = \mathcal{O}(\omega^2 l/\omega^2 r) \ll l/L = \varepsilon$ and we assume $R = \mathcal{O}(1)$. It should be noted that the requirement $R \leqslant \mathcal{O}(1)$ is linked to the hypothesis of separation of scales with regard to excitation. Greater orders of magnitude of R would yield

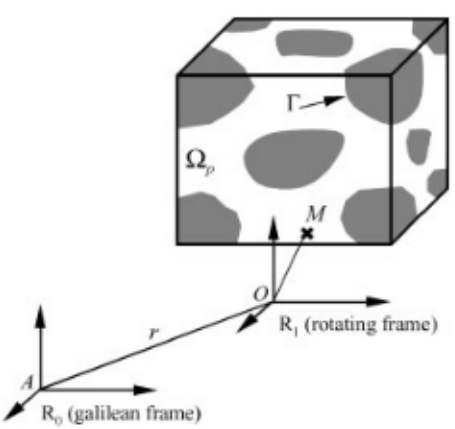

Figure 2. Scheme of the periodic cell Ω in a non-Galilean frame R_1.

non-homogenizable problems, i.e. problems for which there exists no equivalent macroscopic description. To account for Coriolis effects and as noted in the introduction, we assume $\mathsf{Ek} = \mathcal{O}(1)$. For ease of formulation, we again keep, for the dimensionless variables, the same notations as for the original variables. The formal dimensionless set that describes the flow takes the form

$$\mu\nabla^2\mathbf{w} - Q\nabla p = \rho(R\gamma(O) + \mathsf{Ek}^{-1}\boldsymbol{\omega}\times\mathbf{w} + RA\boldsymbol{\omega}\times(\boldsymbol{\omega}\times\mathbf{OM})) \quad \text{in } \Omega_p \tag{28}$$

$$\nabla\cdot\mathbf{w} = 0 \quad \text{in } \Omega_p, \quad \mathbf{w} = \mathbf{0} \quad \text{on } \Gamma \tag{29}$$

4.2. Upscaling

Incorporating expansions (14)–(15) in the set (28)–(29) and identifying at the successive orders of ε, we obtain successive boundary-value problems, which we now have to be solve. As in the preceding section, the lowest order yields

$$\frac{\partial p^{(0)}}{\partial y_i} = 0, \quad p^{(0)} = p^{(0)}(\mathbf{x}) \tag{30}$$

Considering the next order, we obtain the following boundary-value problem of unknowns $\mathbf{w}^{(0)}$ and $p^{(1)}$:

$$\mu\frac{\partial^2 w_i^{(0)}}{\partial y_j\partial y_j} - G_i - Q^*\frac{\partial p^{(1)}}{\partial y_i} = \mathsf{Ek}^{-1}\rho\varepsilon_{ijk}\omega_j w_k^{(0)} \quad \text{in } \Omega_p \tag{31}$$

$$\frac{\partial w_i^{(0)}}{\partial y_i} = 0 \quad \text{in } \Omega_p, \quad w_i^{(0)} = 0 \quad \text{on } \Gamma \tag{32}$$

where $\mathbf{w}^{(0)}$ and $p^{(1)}$ are Ω-periodic and the quantity $Q^* = Q\varepsilon = \mathcal{O}(1)$.

In the above equations, the symbol ε_{ijk} denotes the permutation symbol and the vector $\mathbf{G}$ represents the macroscopic driving force which is independent of $\mathbf{y}$ and which is defined by $\mathbf{G} = Q^*\nabla_x p^{(0)} + R\rho\gamma(O)$, with $\gamma(O) = Ng$, and where the subscript x denotes the derivative with respect to the variable $\mathbf{x}$. Let now multiply Equation (31) by $\mathbf{u}\in W$ and integrate it over Ω_p. Integration by parts and then using the divergence theorem, periodicity, and the boundary condition on Γ, we obtain

$$\forall\mathbf{u}\in W, \quad \int_{\Omega_p}\mu\frac{\partial u_i}{\partial y_j}\frac{\partial w_i^{(0)}}{\partial y_j}\,\mathrm{d}y + \int_{\Omega_p}\mathsf{Ek}^{-1}\rho\varepsilon_{ijk}\omega_j w_k^{(0)}u_i\,\mathrm{d}y = -\int_{\Omega_p}u_i G_i\,\mathrm{d}y \tag{33}$$

Formulation (33) is strongly elliptic, and there exists a unique $\mathbf{w}^{(0)}$ which is a linear vector function of $\mathbf{G}$

$$w_i^{(0)} = -\frac{k_{ij}^{\mathrm{rot}}(\mathsf{Ek}^{-1})}{\mu}G_j \tag{34}$$

where the tensor field $\mathbf{k}^{\mathrm{rot}}$ now depends on both Ek^{-1} and $\mathbf{y}$. Finally, integrating over Ω_p the second order of the volume balance (29), we obtain

$$\frac{\partial v_i}{\partial x_i} = 0, \quad v_i = \langle w_i^{(0)}\rangle = -\frac{K_{ij}^{\mathrm{rot}}(\mathsf{Ek}^{-1})}{\mu}G_j, \quad K_{ij}^{\mathrm{rot}} = \frac{1}{\Omega}\int_{\Omega_p}k_{ij}^{\mathrm{rot}}\,\mathrm{d}y \tag{35}$$

which represents the macroscopic equivalent behaviour at the order $\mathcal{O}(\varepsilon)$ of approximation. From its definition, we see that the filtration tensor $\mathbf{K}^{\mathrm{rot}}(\mathsf{Ek}^{-1})$ depends on the angular velocity $\boldsymbol{\omega}$, the kinetic viscosity μ/ρ and the characteristic length l through the Ekman number.

4.3. Comments

The following essential features of the above-derived modified Darcy's law (35) can be stated:

- As for the macroscopic velocity in Darcy's law, it can be shown [11] that the velocity $\mathbf{v} = \langle \mathbf{w}^{(0)} \rangle$ in (35) is a surface average velocity, that is a Darcy's velocity. It should also be underlined that the physical meaning of the macroscopic pressure is preserved.
- Although formulation (35) is a Darcy's-type law (23), there exist, however, important differences. In effect, it can be shown that the dimensional effective permeability tensor $\mathbf{K}^{\mathrm{rot}}(\mathsf{Ek}^{-1})$ (m^2) which characterize the porous medium at a given Ekman number, is a positive but non-symmetric tensor [7, 8], and that it verifies Hall–Onsager's relationship

$$K_{ij}^{\mathrm{rot}}(\boldsymbol{\omega}) = K_{ji}^{\mathrm{rot}}(-\boldsymbol{\omega}) \tag{36}$$

  which expresses the analogue of Hall's effect for filtration. All these properties directly arise from the weak formulation (33). Obviously, the permeability tensor $\mathbf{K}^{\mathrm{rot}}(\mathsf{Ek}^{-1})$ can be put in the form

$$\mathbf{K}^{\mathrm{rot}} = \mathbf{K} \cdot \mathbf{E}(\mathsf{Ek}^{-1}) \tag{37}$$

  where $\mathbf{K}$ (m^2) is the classical intrinsic permeability tensor and $\mathbf{E}(\mathsf{Ek}^{-1})$ (dimensionless) is a positive but non-symmetric second-order tensor which depends on the Ekman number only and, which verifies the Hall–Onsager's relation $E_{ij}(\boldsymbol{\omega}) = E_{ji}(-\boldsymbol{\omega})$.
- The permeability tensor of an isotropic porous medium of Galilean permeability K and submitted to an angular velocity $\boldsymbol{\omega} = \omega \mathbf{e}_3$ takes the form

$$\mathbf{K}^{\mathrm{rot}} = \begin{pmatrix} K_{11}^{\mathrm{rot}}(\omega) & K_{12}^{\mathrm{rot}}(\omega) & 0 \\ -K_{12}^{\mathrm{rot}}(\omega) & K_{11}^{\mathrm{rot}}(\omega) & 0 \\ 0 & 0 & K \end{pmatrix} \tag{38}$$

  Note that the tensor $\mathbf{K}^{\mathrm{rot}}$ is invariant under any rotation of $\mathbf{e}_3$ axis. Therefore, the principal components of $\mathbf{K}^{\mathrm{rot}}$ are complex valued.
- Rotation effects are twofold. Firstly, the centrifugal force increases the forcing term ∇p, which is the sought-after purpose in a centrifuge filtration test. Compared to a classical filtration test, this increased forcing term does not change the pore-scale velocity pattern: velocities are just everywhere increased by a constant ratio. Permeability tensor is not affected by the centrifugal force itself. Secondly, Coriolis forces deviate the pore-scale velocity field, which results in a rotation-dependent permeability. This second effect is present when the Ekman number is $\mathcal{O}(1)$. How the permeability tensor is affected by the rotation is measured by the value of Ek^{-1}.

4.4. Is the non-inertial flow law applicable to centrifuge tests?

The above analysis is conducted under three conditions that are related to the dimensionless numbers that enter the Stokes equation which describes the flow at the pore scale. The first

condition concerns the ratio of the macroscopic convective inertia to the viscous term

$$R = \frac{|\rho\gamma(O)|}{|\mu\nabla^2\mathbf{w}|} = \frac{\rho\omega^2 r l^2}{\mu w} = \mathcal{O}(1) \tag{39}$$

Recall that a quantity Φ is $\mathcal{O}(1)$ if $\varepsilon \ll \Phi \ll \varepsilon^{-1}$. Coriolis effects will be seen if Ekman number is $\mathcal{O}(1)$

$$\mathsf{Ek} = \frac{|\mu\nabla^2\mathbf{w}|}{|2\rho\boldsymbol{\omega}\times\mathbf{w}|} = \frac{\mu}{2\rho\omega l^2} = \mathcal{O}(1) \tag{40}$$

In the analysis, we have neglected non-linear terms in the stokes equation, that yields a macroscopic linear flow law. It is generally admitted that the validity of such a linear law is for pore Reynolds number equal or less than 10 [12]. Therefore, the third condition writes

$$Re = \frac{\rho w l}{\mu} \leqslant 10 \tag{41}$$

It is also of interest to introduce the ratio D of the Coriolis inertia to the centrifugal force [14]

$$D = \frac{|2\rho\boldsymbol{\omega}\times\mathbf{w}|}{|\rho\gamma(O)|} = \frac{2w}{r\ \omega} = R^{-1}\mathsf{Ek}^{-1} = \mathcal{O}(1) \tag{42}$$

In (42), the product $r\ \omega$ represents the velocity of the centrifuge basquet. If a typical value of D in a centrifuge test is 10^{-3}, to be consistent with the theory, we should have $\varepsilon \ll 10^{-3}$, which means a very good separation of scales. From (39), (40) and (41), we have

$$\omega \leqslant \frac{800\mu}{\rho r^2}\frac{\mathsf{Ek}}{D^2} \tag{43}$$

If we consider a centrifuge test with $r = 5$ m, water, $\mathsf{Ek} = 1$ and $D = 10^{-3}$, that gives $\omega \leqslant 32$, which is quite consistent.

As an example, consider the test reported in Reference [2] on a sand sample. In this experiment, $r = 5.5$ m, and the filtrating liquid is water, with $\mu = 10^{-3}$ Pa .s and $\rho = 10^3$ kg/m^3. For the maximum reported centrifugal acceleration, $r\omega^2 = 50$ g, the fluid velocity is $w \approx 0.01$ m/s. That gives $D \approx 4 \times 10^{-4}$. The main difficulty stands in the evaluation of the pore characteristic size l. Firstly, let us adopt d_{50} as an evaluation of l: $l \approx 0.2$ mm. That gives $\mathsf{Ek}^{-1} \approx 0.75$ and $Re \approx 2$. We deduce that Coriolis effects are seen and the linear seepage law is valid. The decreasing permeability with increasing ω in Reference [2] could be due to this effect, although experimental data were obtained using the classical Darcy's law in place of the non-inertial flow law. Secondly, it could be more pertinent to estimate l as the characteristic thickness of the narrowings between sand grains, which are the main contributors to permeability coefficient as in Reference [5]. The sand sample shows an isotropic permeability at rest $K = 2.4 \times 10^{-11}$ m^2. Therefore, we now adopt $l \approx \sqrt{K} \approx 5 \times 10^{-6}$ m. That yields $\mathsf{Ek}^{-1} \approx 5 \times 10^{-4}$, which shows that Coriolis effects are quite negligible. To overcome this difficulty to estimate l, numerical investigations of Coriolis effects on the permeability of a periodic square of cylinders and spheres are presented in Section 5.

4.5. *Comparison between* $\mathbf{K}^{\mathrm{rot}}$ *and* $\mathbf{K}^{\mathrm{phe}}$

Considering two distinct simple pore geometries which are saturated by water ($\mu = 10^{-3}$ Pa s, $\rho = 10^3$ kg/m^3), we have plotted the evolution of the dimensionless permeabilities $K_{11}^{\mathrm{rot}}(\omega)/K_{11}^{\mathrm{rot}}(0)$ and $K_{21}^{\mathrm{rot}}(\omega)/K_{11}^{\mathrm{rot}}(0)$ with respect to the angular velocity ω (see curves (i) and

(ii) in Figures 3 and 4. These figures also show the profiles of $K_{11}^{\mathrm{phe}}(\omega)$ and $K_{21}^{\mathrm{phe}}(\omega)$ (see curves (iii) and (iv)). As already mentioned, both tensors $\mathbf{K}^{\mathrm{rot}}$ and $\mathbf{K}^{\mathrm{phe}}$ account for Coriolis forces and verify Hall–Onsager's relationship (36). It can be seen from Figures 3 and 4, that $K_{11}^{\mathrm{phe}}(\omega)$ and $K_{21}^{\mathrm{phe}}(\omega)$ keep the same profiles on both geometries: we may thus conclude that the Coriolis correction in $\mathbf{K}^{\mathrm{phe}}$ is independent of pore geometry. In the case of parallel plane fissures (Figure 3), we observe that the tensor $\mathbf{K}^{\mathrm{phe}}$ provides a good approximation of $\mathbf{K}^{\mathrm{rot}}$. On the other hand, in the case of a bundle of capillaries, the profiles of $\mathbf{K}^{\mathrm{rot}}$ tells us that the Coriolis forces have no impact on the filtration process. This is due to the fact that the pore surface prevents the Coriolis force from acting on fluid flow. Figure 4 clearly shows that $\mathbf{K}^{\mathrm{phe}}$ fails at reproducing this effect.

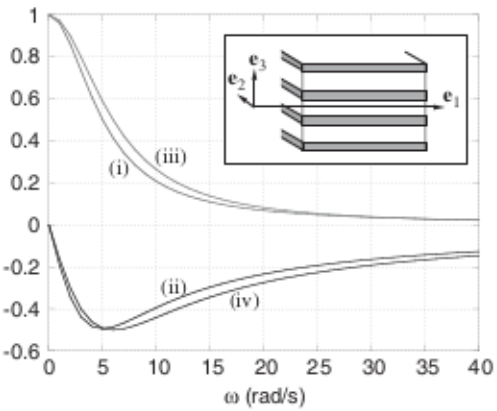

Figure 3. Network of parallel plane fissures saturated by water. Dimensionless permeabilities versus angular velocity $\boldsymbol{\omega} = \omega \mathbf{e}_3$: (i) $K_{11}^{\mathrm{rot}}(\omega)/K_{11}^{\mathrm{rot}}(0)$; (ii) $K_{21}^{\mathrm{rot}}(\omega)/K_{11}^{\mathrm{rot}}(0)$; (iii) $K_{11}^{\mathrm{phe}}(\omega)$; and (iv) $K_{21}^{\mathrm{phe}}(\omega)$.

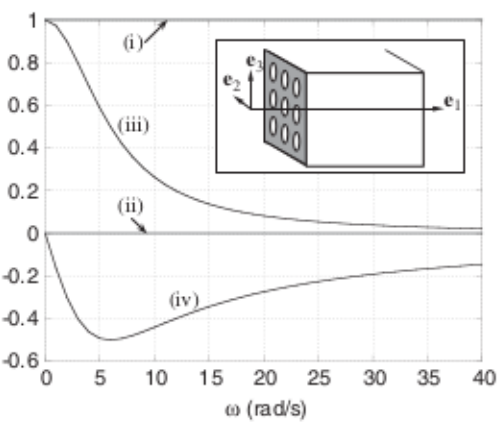

Figure 4. Bundle of capillaries saturated by water. Dimensionless permeabilities of a porous medium versus angular velocity $\boldsymbol{\omega} = \omega \mathbf{e}_3$: (i) $K_{11}^{\mathrm{rot}}(\omega)/K_{11}^{\mathrm{rot}}(0)$; (ii) $K_{21}^{\mathrm{rot}}(\omega)/K_{11}^{\mathrm{rot}}(0)$; (iii) $K_{11}^{\mathrm{phe}}(\omega)$; and (iv) $K_{21}^{\mathrm{phe}}(\omega)$.

5. NUMERICAL INVESTIGATIONS OF CORIOLIS EFFECTS ON THE FLOW THROUGH ROTATING POROUS MEDIA

The objective of this last section is to highlight the influence of the Coriolis forces on the flow in rotating porous media. For this purpose, firstly we investigate the influence of Coriolis force on the flow at the microscopic scale, i.e. on the permeability of a periodic array of cylinders and spheres. Secondly, we study the flow at the macroscopic scale, i.e. through a permeameter placed in a centrifuge basket.

5.1. Determination of the permeability tensor $\mathbf{K}^{\mathrm{rot}}(\omega)$

5.1.1. Square array of cylinders. The porous medium consists of a periodic array of cylinders (Figure 5(a)) which is placed in a centrifuge at constant angular velocity $\boldsymbol{\omega} = \omega \mathbf{e}_3$. The radius of the cylinder is a and e is the size of the periodic cell. Thus, the porosity of the porous medium $\phi = 1 - (\pi a^2)/e^2$ varies from 0.215 to 1. We suppose that the porous medium is submitted to a macroscopic gradient $\mathbf{G} = G_2 \mathbf{e}_2$, which is due to the centrifuge acceleration only,

$$\mathbf{G} = \rho r \omega^2 \mathbf{e}_2 = \rho N g \mathbf{e}_2 \tag{44}$$

where ρ is the water density, r denotes the radius of the centrifuge and N represents the acceleration level. As a result of the simplified geometry and macroscopic pressure gradient, the flow through the porous medium reduces to a 2D problem within the plane $(\mathbf{e}_1, \mathbf{e}_2)$. The permeability tensor $\mathbf{K}^{\mathrm{rot}}(\omega)$ of the periodic array of cylinders takes the form

$$\mathbf{K}^{\mathrm{rot}} = \begin{pmatrix} K_{11}^{\mathrm{rot}}(\omega) & -K_{21}^{\mathrm{rot}}(\omega) & 0 \\ K_{21}^{\mathrm{rot}}(\omega) & K_{11}^{\mathrm{rot}}(\omega) & 0 \\ 0 & 0 & K_{33} \end{pmatrix} \tag{45}$$

The permeability tensor $\mathbf{K}^{\mathrm{rot}}(\omega)$ is obtained by solving the boundary-value problem (31)–(32) in its dimensional forms over the periodic cell, in which the unknowns, namely the microscopic velocity field $\mathbf{w}^{(0)}$ and the local pressure $p^{(1)}$ are Ω-periodic. We have also considered that

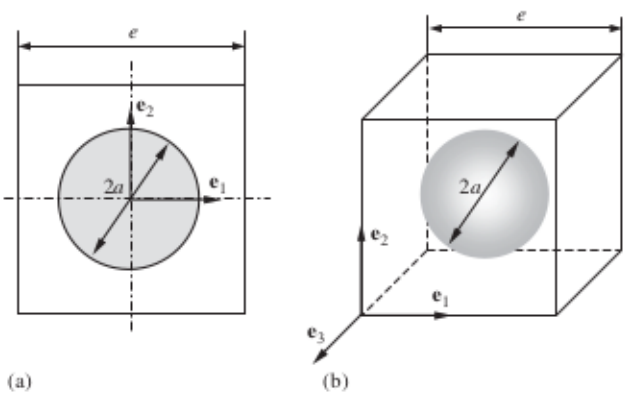

Figure 5. Characteristic dimensions of the periodic cell: (a) periodic array of cylinders; and (b) periodic array of spheres.

$\mu = 10^{-3}$ Pa s and $\rho = 10^3$ kg/m^3. The macroscopic driving force $\mathbf{G}$ is determined by the value of ω under consideration. The permeabilities of the porous medium are then deduced from Equations (34) and (35). We have solved the above-mentioned boundary-value problem for each value of ω, by using a finite element code [15].

Figure 6 shows the microscopic velocity fields $\mathbf{w}^{(0)}$ which we have obtained for four different values of the angular velocity ω and for a given value of porosity $\phi = 0.7$. We observe that the flow deviations due to Coriolis forces increase with increasing angular velocity ω. The plots of the dimensionless permeabilities $K_{11}^{\mathrm{rot}}(\omega)/K_{11}^{\mathrm{rot}}(0)$ and $K_{21}^{\mathrm{rot}}(\omega)/K_{11}^{\mathrm{rot}}(0)$ with respect to ω for three different values of porosity ϕ (0.9, 0.7 and 0.5) and for two values of e (2 and 1.5 mm) are shown in Figure 7(a). For a given angular velocity, we observe that Coriolis effects on the permeability decrease with decreasing the porosity ϕ and with decreasing the length e. Finally, Figure 7(b) shows the evolution of all these numerical results with respect to the inverse of Ekman number defined as

$$\mathrm{Ek}^{-1} = 2\rho\omega \frac{K_{11}^{\mathrm{rot}}(0)}{\mu} \tag{46}$$

where we note that the characteristic length l in use to calculate Ek is $\sqrt{K_{11}^{\mathrm{rot}}(0)}$. This figure shows that dimensionless permeabilities $K_{11}^{\mathrm{rot}}(\omega)/K_{11}^{\mathrm{rot}}(0)$ and $K_{21}^{\mathrm{rot}}(\omega)/K_{11}^{\mathrm{rot}}(0)$ can be adjusted by a

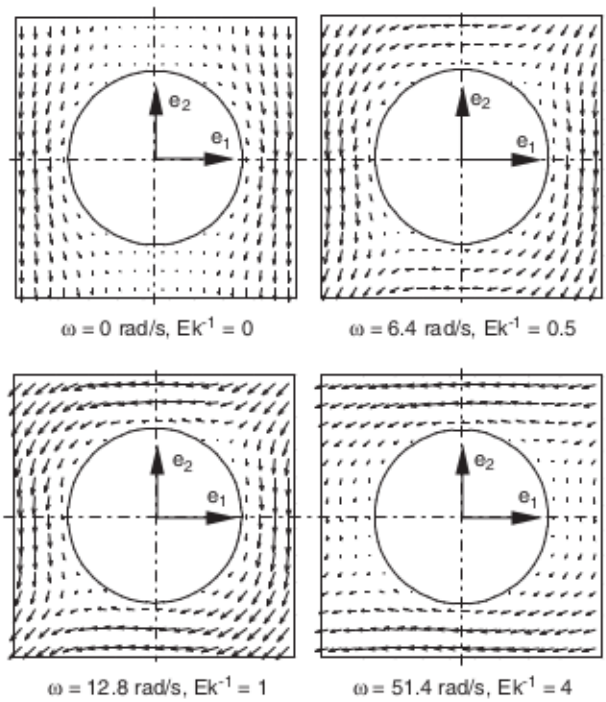

Figure 6. Microscopic velocity field $\mathbf{w}^{(0)}$ versus angular velocity $\boldsymbol{\omega} = \omega\mathbf{e}_3$, i.e. Ek^{-1} defined by (46). The macroscopic driving pressure gradient is $\mathbf{G} = G_2\mathbf{e}_2$. The porosity ϕ is equal to 0.7.

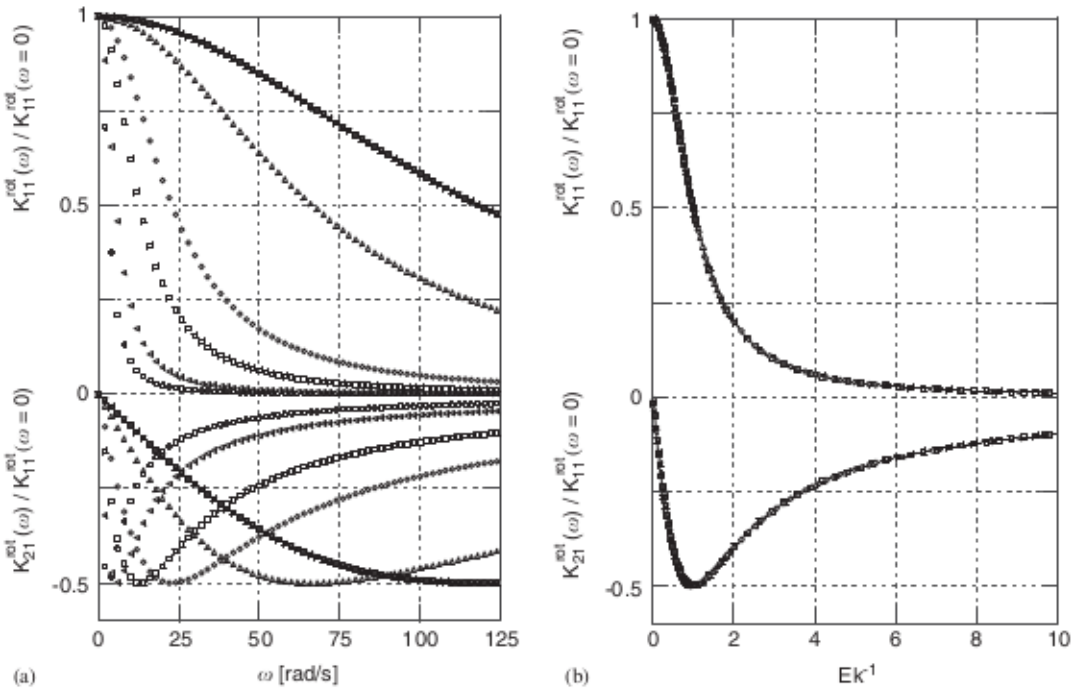

Figure 7. Periodic array of cylinders: dimensionless permeabilities $K_{11}^{rot}(\omega)/K_{11}^{rot}(0)$ and $K_{21}^{rot}(\omega)/K_{11}^{rot}(0)$ versus angular velocity ω (a) and versus Ek^{-1} defined by (46) (b), for three different values of porosity ϕ and for two values of e: ($\bigcirc$) $\phi = 0.9$, $e = 2$ mm, ($\square$) $\phi = 0.7$, $e = 2$ mm, ($\triangle$) $\phi = 0.5$, $e = 2$ mm, ($\triangleleft$) $\phi = 0.9$, $e = 1.5$ mm, ($\diamond$) $\phi = 0.7$, $e = 1.5$ mm, ($\boxtimes$) $\phi = 0.5$, $e = 1.5$ mm. The continuous line represents Equation (47).

unique curve which depends on the Ekman number in form (46) only,

$$K_{11}^{rot}(\omega) = K_{11}^{rot}(0)\frac{1}{1+(Ek^{-1})^2}, \quad K_{21}^{rot}(\omega) = K_{11}^{rot}(0)\frac{-Ek^{-1}}{1+(Ek^{-1})^2} \tag{47}$$

These relations are plotted in Figure 7(b) (continuous line). In this particular case, it can be shown that relations (47) are consistent with the phenomenological model (6). That is not the case if $\boldsymbol{\omega} \neq \omega \mathbf{e}_3$. Finally, the above numerical results on the flow through a periodic array of cylinders clearly show that it is more pertinent to use the permeability to evaluate the Ekman number.

5.1.2. Square array of spheres. Now, the porous medium under consideration consists of a cubic array of spheres (Figure 5(b)) which is placed in a centrifuge at constant angular velocity $\boldsymbol{\omega} = \omega \mathbf{e}_3$. The radius of the sphere is a and e is the size of the periodic cell. The porosity of the porous medium $\phi = 1 - (4\pi a^3/3)/e^3$ varies from 0.476 to 1. Once again, we suppose that the medium is submitted to the same macroscopic gradient $\mathbf{G} = G_2 \mathbf{e}_2 = \rho r \omega^2 \mathbf{e}_2$, which is due to the centrifuge acceleration only. As a result of the geometry and macroscopic pressure gradient,

the permeability tensor $\mathbf{K}^{\mathrm{rot}}(\omega)$ of the cubic array of spheres takes the form

$$\mathbf{K}^{\mathrm{rot}} = \begin{pmatrix} K_{11}^{\mathrm{rot}}(\omega) & -K_{21}^{\mathrm{rot}}(\omega) & 0 \\ K_{21}^{\mathrm{rot}}(\omega) & K_{11}^{\mathrm{rot}}(\omega) & 0 \\ 0 & 0 & K_{33} \end{pmatrix} \tag{48}$$

with $K_{33} = K_{11}^{\mathrm{rot}}(0)$. Numerical values of the permeability tensor $\mathbf{K}^{\mathrm{rot}}(\omega)$ have been obtained by following the same methodology presented in Section 5.1.1.

The plots of the dimensionless permeabilities $K_{11}^{\mathrm{rot}}(\omega)/K_{11}^{\mathrm{rot}}(0)$ and $K_{21}^{\mathrm{rot}}(\omega)/K_{11}^{\mathrm{rot}}(0)$ with respect to ω for three different values of porosity ϕ (0.9, 0.7 and 0.5) and for two values of e (2 and 1.5 mm) are shown in Figure 8(a). Once again, for a given angular velocity, we observe that Coriolis effects on the permeability decrease with decreasing the porosity ϕ and with decreasing the length e. Finally, Figure 8(b) shows the evolution of all these numerical results with respect to Ek^{-1} defined by Equation (46). In this case, we obtained three different curves $K_{11}^{\mathrm{rot}}(\omega)/K_{11}^{\mathrm{rot}}(0)$ and $K_{21}^{\mathrm{rot}}(\omega)/K_{11}^{\mathrm{rot}}(0)$ which depend on the Ekman number and the porosity. Relations (47), which are consistent with the phenomenological model (6), have been also plotted in Figure 8(b). These relations are not capable to describe our numerical data. This result confirms that

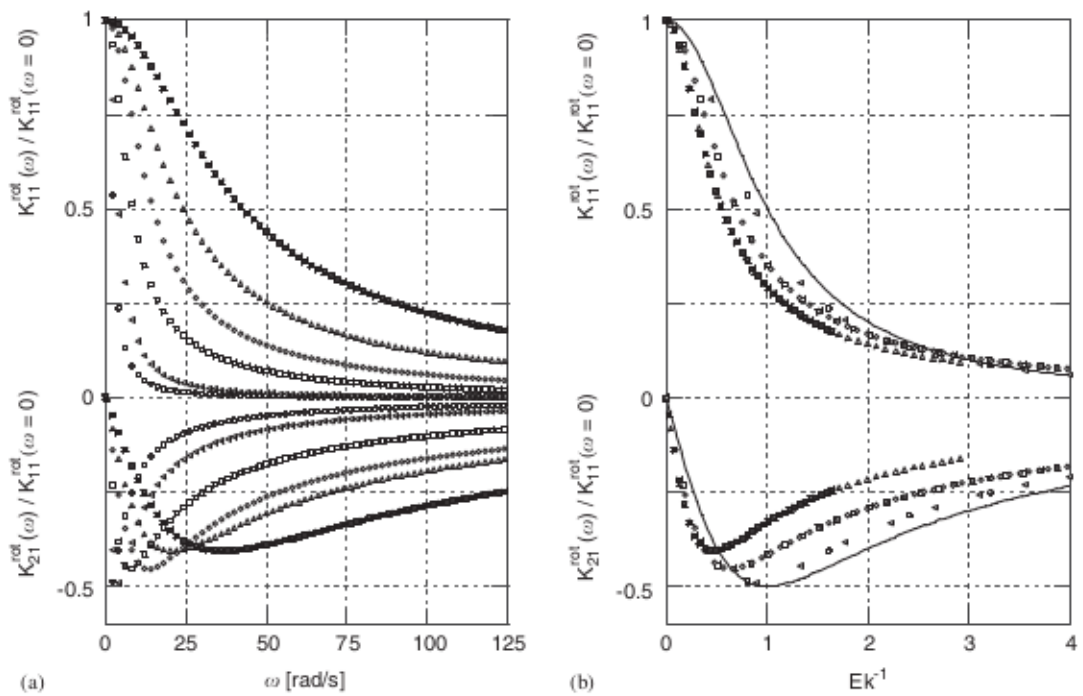

Figure 8. Periodic array of spheres: dimensionless permeabilities $K_{11}^{\mathrm{rot}}(\omega)/K_{11}^{\mathrm{rot}}(0)$ and $K_{21}^{\mathrm{rot}}(\omega)/K_{11}^{\mathrm{rot}}(0)$ versus angular velocity ω (a) and versus Ek^{-1} defined by (46) (b), for three different values of porosity ϕ and for two values of e: ($\bigcirc$) $\phi = 0.9$, $e = 2$ mm, ($\square$) $\phi = 0.7$, $e = 2$ mm, ($\triangle$) $\phi = 0.5$, $e = 2$ mm, ($\triangleleft$) $\phi = 0.9$, $e = 1.5$ mm, ($\Diamond$) $\phi = 0.7$, $e = 1.5$ mm, ($\boxtimes$) $\phi = 0.5$, $e = 1.5$ mm. The continuous line represents Equation (47).

model (6) fails at reproducing three-dimensional Coriolis effects which can appear in all types of pore geometry.

5.2. 2D-flow simulations in a rotating permeameter

The objective of this last section is to highlight the influence of the Coriolis forces on the flow in a rotating porous medium at the macroscopic scale. For this purpose, we consider a permeameter which is placed in a centrifuge at constant angular velocity $\boldsymbol{\omega} = \omega \mathbf{e}_3$ (Figure 9). The characteristic dimensions of the permeameter are L and H. The porous medium consists of a periodic array of cylinders. It is submitted to a macroscopic gradient $\mathbf{G} = G_2 \mathbf{e}_2 = ((p_0 - p_1)/H)\mathbf{e}_2$, where p_0 and p_1 $(p_0 > p_1)$ are the inlet and outlet imposed pressures, respectively. We have also considered impervious lateral surfaces. As a result of the simplified geometry and macroscopic pressure gradient, the flow through the permeameter reduces to a 2D problem within the plane $(\mathbf{e}_1, \mathbf{e}_2)$. By making use of the above determination of the permeability $\mathbf{K}^{\mathrm{rot}}(\omega)$ (47) and by considering appropriate macroscopic boundary conditions, we have solved model (35) and performed 2D-flow simulations by means of the same finite element code [15].

Figure 10 shows the macroscopic velocity field $\mathbf{v} = \langle \mathbf{w}^{(0)} \rangle$ and the contours of the dimensionless pressure field $((p - p_1)/(p_0 - p_1))$ obtained for three different values of the inverse of Ekman number (46) when the ratio $H/L = 2$. We observe that flow deviations due Coriolis forces increase with increasing values of Ek^{-1}, i.e. increasing ω and that the pressure field is not homogeneous.

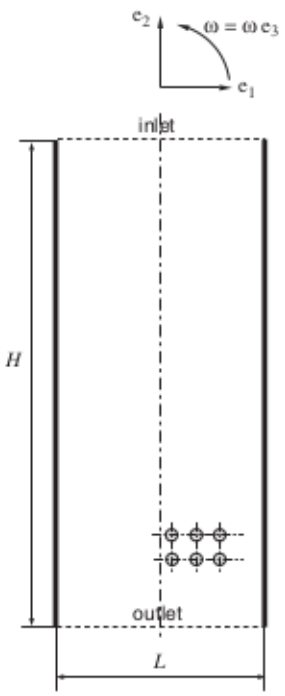

Figure 9. Cross-section of a permeameter placed in a centrifuge at angular velocity $\boldsymbol{\omega} = \omega \mathbf{e}_3$.

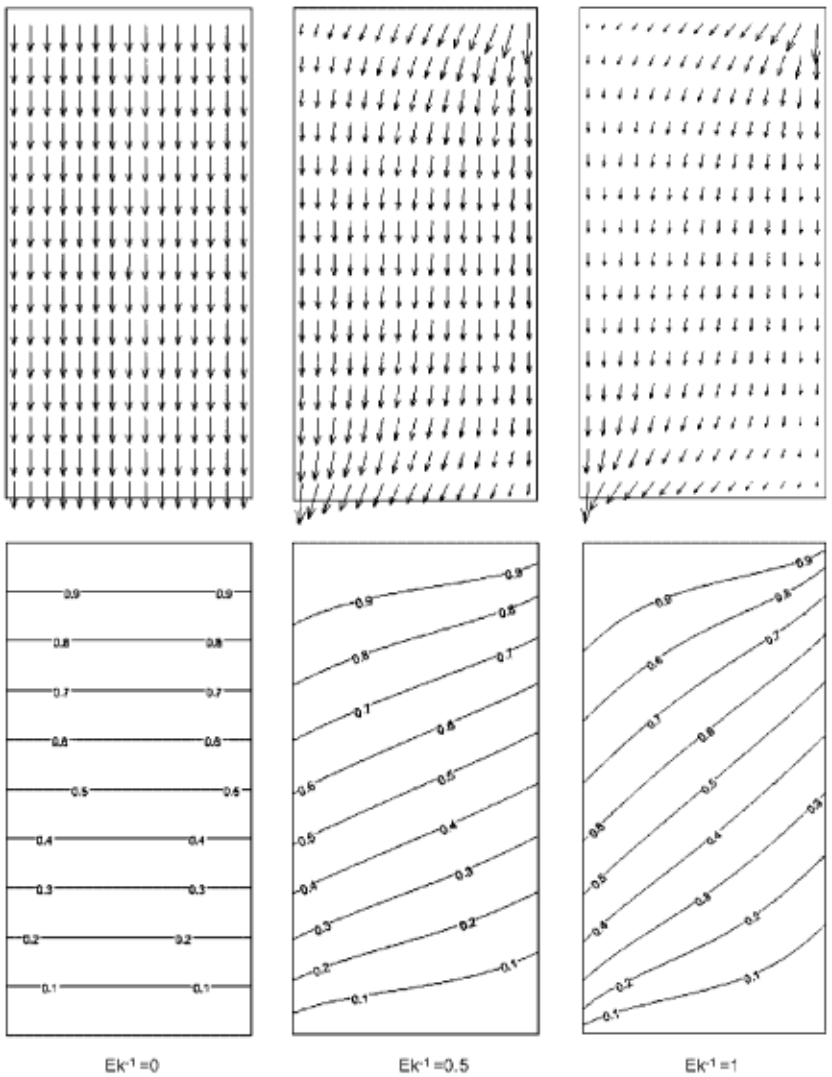

Figure 10. Flow in a permeameter placed in a centrifuge: macroscopic velocity field $\mathbf{v} = \langle \mathbf{w}^{(0)} \rangle$ and contours of the dimensionless pressure field $((p - p_1)/(p_0 - p_1))$ obtained for three different values of Ek^{-1} defined by Equation (46) in the case where the ratio $H/L = 2$.

Centrifuge test data which are available in the literature are usually performed on isotropic porous media. With the view to compare the classical interpretation of centrifuge tests to our results, let us introduce the scalar parameter K^{cen} (m^2) ($\neq k^{\mathrm{cen}}$ see (3)) defined by the classical Darcy's law,

$$\mathbf{v} = -\frac{K^{\mathrm{cen}}}{\mu}\mathbf{G} \tag{49}$$

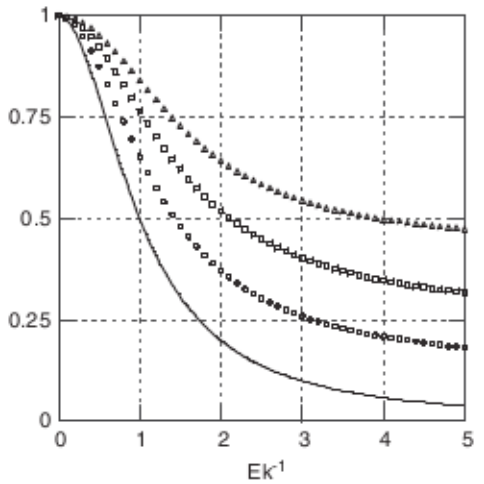

Figure 11. Flow in a permeameter placed in a centrifuge: $K^{cen}(\omega)/K_{11}^{rot}(0)$ with respect to Ek^{-1} (46) for three different values of the ratio H/L. ($\bigcirc$) $H/L = 1$, ($\square$) $H/L = 2$, ($\triangle$) $H/L = 4$. The continuous line represents $K_{11}^{rot}(\omega)/K_{11}^{rot}(0)$ (47).

Parameter K^{cen} can be obtained from our numerical data

$$K^{cen}(\omega) = \frac{\mu Q(\omega) H}{L(p_0 - p_1)} \tag{50}$$

where $Q(\omega)$ (m^2/s) is the flow rate in the permeameter which depends on the value of ω under consideration, i.e. Ek^{-1}. Figure 11 shows the plots of the dimensionless permeabilities $K^{cen}(\omega)/K_{11}^{rot}(0)$ with respect to Ek^{-1} (46) for three different values of the ratio H/L (1, 2 and 4). The dimensionless permeability $K_{11}^{rot}(\omega)/K_{11}^{rot}(0)$ defined by Equation (47) is also plotted in Figure 11. The curves of the evolution of $K^{cen}(\omega)/K_{11}^{rot}(0)$ with respect to Ek^{-1} clearly show that $K^{cen}(\omega) \neq K_{11}^{rot}(\omega)$ and prove that $K^{cen}(\omega)$, which depends on the ratio H/L, is not intrinsic. We observe that Coriolis effects may lead to significant variations of the permeability K^{cen} during centrifuge tests when the Ekman number is $\mathcal{O}(1)$. These variations also strongly depends on the ratio H/L. We can note that if $\mathsf{Ek}^{-1} < 0.2$, which is the case of geotechnical centrifuge tests reported in Reference [2], Coriolis effects are quite negligible,

$$\frac{K^{cen} - K_{11}^{rot}(0)}{K_{11}^{rot}(0)} \leqslant 5\% \tag{51}$$

The above observations prove that existing experimental data are not sufficient for determining an experimental tensor $\mathbf{K}^{rot}$. In effect, the knowledge of $\mathbf{K}^{rot}$ would require the measurement of two parameters, namely K_{11}^{rot} and K_{21}^{rot} and none of them is equal to K^{cen}, which can be actually measured during centrifuge tests.

6. CONCLUSIONS

We have revisited the filtration law for fluid flow in rotating porous media, by applying homogenization to the pore-scale physical description. The derived filtration law is a modified

Darcy's law. We have shown that in rotating porous media Coriolis forces may lead to significant flow deviations. In effect, these forces give rise to a non-symmetric tensor of permeability $\mathbf{K}^{\mathrm{rot}}$, which depends upon the angular velocity. We have proved that this tensor verifies Hall–Onsager's relationship

$$K_{ij}^{\mathrm{rot}}(\boldsymbol{\omega}) = K_{ji}^{\mathrm{rot}}(-\boldsymbol{\omega})$$

which expresses the analogue for filtration of Hall's effect. This latter property also proves that, under rotation, the effective permeability of an isotropic porous medium is a non-isotropic tensor. All the above-mentioned effects and properties become significant provided the Ekman number, $\mathsf{Ek} = \mu/2\rho\omega l^2$ is $\mathcal{O}(1)$.

Numerical simulations have been performed to highlight the influence of the Coriolis forces on the flow in a rotating porous medium at both the microscopic and the macroscopic scales, i.e. on the permeability of a periodic array of cylinders or spheres and on the flow through a permeameter placed in a centrifuge basket. Our numerical results clearly show the flow deviations due to Coriolis forces at both the pore scale and the sample scale. We have shown that, the tensor of the phenomenological model, $\mathbf{K}^{\mathrm{phe}}$ includes Coriolis effects and verifies Hall–Onsager's relationship, but that this Coriolis correction fails at reproducing the flow for all types of pore geometry. Numerical results obtained for different values of the radius of cylinders (or spheres) and porosity are presented. Both cases suggest that it is more pertinent to use the permeability to estimate the Ekman number. Finally, numerical simulations on the flow through a permeameter placed in a centrifuge basket show that Coriolis effects may lead to significant variations of the permeability K^{cen} during centrifuge tests when the Ekman number is $\mathcal{O}(1)$. These variations are estimated to be less than 5% if $\mathsf{Ek}^{-1} < 0.2$, which is the case for classical geotechnical centrifuge tests. The key parameter to measure eventual Coriolis effects is the Ekman number. Ekman number is different from the ratio D of the fluid velocity to the basket velocity (see (42)) which is generally used to measure such effects [14].

The determination of the effective tensor $\mathbf{K}^{\mathrm{rot}}(\omega)$ requires the knowledge of two parameters: K_{11}^{rot} and K_{21}^{rot}. Therefore, $\mathbf{K}^{\mathrm{rot}}(\omega)$ cannot be determined from existing experimental data, since they are based on the single measurement of K^{cen}. Further developments of the present work should therefore include the experimental determination of K_{11}^{rot} and K_{21}^{rot}.

Finally, let us remark that in some industrial applications, like centrifugal casting, Coriolis effects on the flow through the mushy zone which appear during the solidification process are not negligible. During such a process, the typical angular velocity is 500 rpm. Considering, a dynamic viscosity of the metallic liquid $\mu \approx 10^{-3}$ Pa s, a density $\rho \approx 7.3 \times 10^3$ kg/m^3 and a permeability K of the mushy zone which may vary between 10^{-8} and 10^{-14} m^2 [16], we have $0 \leqslant \mathsf{Ek}^{-1} \leqslant 4$.

REFERENCES

1. Singh DN, Gupta AK. Modelling hydraulic conductivity in a small centrifuge. *Canadian Geotechnical Journal* 2000; **37**:1150–1155.
2. Khalifa A, Garnier J, Thomas P, Rault G. Scaling laws of water flow in centrifuge models. In *International Symposium on Physical Modelling and Testing in Environmental Geotechnics (Paris, France)*, Thorel L, Garnier J, Haza E (eds), LCPC: La Baule, 2000; 207–216.
3. Singh DN, Gupta AK. Modelling hydraulic conductivity in a small centrifuge: reply. *Canadian Geotechnical Journal* 2002; **39**:488–489.

4. Robinson RG. Modelling hydraulic conductivity in a small centrifuge: discussion. *Canadian Geotechnical Journal* 2002; **39**:486–487.
5. Vadasz P. Fluid flow through heterogeneous porous media in a rotating square channel. *Transport in Porous Media* 1993; **12**:43–54.
6. de Groot SR, Mazur P. *Non-equilibrium Thermodynamics*. North-Holland: Amsterdam, 1969.
7. Auriault J-L, Geindreau C, Royer P. Filtration law in rotating porous media. *Comptes Rendus de l Academie des Sciences Paris* 2000; **T.328, Serie IIb**:779–784.
8. Auriault J-L, Geindreau C, Royer P. Coriolis effects on filtration law in rotating porous media. *Transport in Porous Media* 2002; **48**:315–330.
9. Bensoussan A, Lions J-L, Papanicolaou G. *Asymptotic Analysis for Periodic Structures*. North-Holland: Amsterdam, 1978.
10. Sanchez-Palencia E. *Non-homogeneous Media and Vibration Theory*. Lectures Notes in Physics, vol. 127. Springer: Berlin, 1980.
11. Auriault J-L. Heterogeneous medium is an equivalent description possible? *International Journal of Engineering Science* 1991; **29**:785–795.
12. Bear J. *Dynamics of Fluids in Porous Media*. Dover: New York, 1972.
13. John J. *Partial Differential Equations*. Springer: Berlin, 1970.
14. Taylor RN. *Geotechnical Centrifuge Technology*. Blackie Academic and Professional: London, 1995.
15. FEMLAB, *Reference Manual, version 2.3. http://www.femlab.com*, 2002.
16. Beckermann C, Wang CY. Multiphase/-scale modelling of alloy solidification. *Annual Review of Heat Transfer* 1995; **6**:115–198.